Pacific Ocean forcing and atmospheric variability are the dominant causes of spatially widespread droughts in the contiguous United States

Seung H. Baek*

Lamont-Doherty Earth Observatory, Columbia University, Palisades, and Department of Earth and Environmental Sciences, Columbia University, New York, New York

Jason E. Smerdon

Lamont-Doherty Earth Observatory, Columbia University, Palisades, New York

Richard Seager

Lamont-Doherty Earth Observatory, Columbia University, Palisades, New York

A. Park Williams

Lamont-Doherty Earth Observatory, Columbia University, Palisades, New York

Benjamin I. Cook

NASA Goddard Institute for Space Studies, New York, and Lamont-Doherty Earth Observatory, Columbia University, Palisades, New York

*Corresponding author:
Seung H. Baek
61 Route 9W
Oceanography 205E
Palisades, NY 10964
Email: sbaek@ldeo.columbia.edu

Key Points

- Models forced with observed sea surface temperatures replicate spatially widespread summer droughts over the contiguous United States.
- Variability in the tropical Pacific explains almost all the ocean forcing of these droughts in the models. The Atlantic plays an ambiguous role.
- Contributions to these droughts from internal atmospheric variability are roughly equal to or greater than the collective ocean forcing.

Abstract

The contributions of oceanic and atmospheric variability to spatially widespread summer droughts in the contiguous United States (hereafter, pan-CONUS droughts) are investigated using 16-member ensembles of the Community Climate Model version 3 (CCM3) forced with observed sea surface temperatures (SSTs) from 1856 to 2012. The employed SST forcing fields are either (i) global or restricted to the (ii) tropical Pacific or (iii) tropical Atlantic to isolate the impacts of these two ocean regions on pan-CONUS droughts. Model results show that SST forcing of pan-CONUS droughts originates almost entirely from the tropical Pacific because of atmospheric highs from the northern Pacific to eastern North America established by La Niña conditions, with little contribution from the tropical Atlantic. Notably, in all three model configurations, internal atmospheric variability influences pan-CONUS drought occurrence by as much or more than the ocean forcing and can alone cause pan-CONUS droughts by establishing a dominant high centered over the US montane West. Similar results are found for the Community Atmosphere Model version 5 (CAM5). Model results are compared to the observational record, which supports model-inferred contributions to pan-CONUS droughts from La Niñas and internal atmospheric variability. While there may be an additional association with warm Atlantic SSTs in the observational record, this association is ambiguous due to the limited number of observed pan-CONUS. The ambiguity thus opens the possibility that the observational results are limited by sampling over the 20th-century and not at odds with the suggested dominance of Pacific Ocean forcing in the model ensembles.

1. Introduction

Droughts in the contiguous United States (CONUS) are common, but spatially widespread droughts that span most of CONUS (herein pan-CONUS droughts) stand out as prominent events, pose significant and specific challenges, and happen less frequently than events that are confined to smaller regions. Pan-CONUS droughts claim higher costs when compared to localized droughts of similar severity because, by definition, they impact more areas while also reducing redundancies in associated water or agricultural resources that might act to mitigate more regionalized events. For instance, the 1988 US drought ranked among the most spatially extensive in recent history and cost the US $40 billion, largely in agricultural losses (Trenberth et al. 1988; Kogan 1995; Andreadis et al. 2005; Rippey 2015). Similarly, the 2012 US drought, which covered over 60% of CONUS (NCDC 2013) and is the most recent pan-CONUS drought, cost the US an estimated $30 billion, again largely in agricultural losses (Rippey 2015). Pan-CONUS droughts occur an average of 21 times per century and have been a consistent feature of US hydroclimate as recorded in moisture-sensitive tree-ring records over the last millennium (e.g. Cook et al. 2014). Understanding the causes, characteristics, and dynamics of these droughts is thus important for developing adaptation strategies and defining their potentially changing frequency and severity in a warming climate.

Characterizing spatial and temporal variability in CONUS drought conditions begins with an understanding of the oceanic influences. Cold Pacific conditions (Ropelewski and Halpert 1986; Gershunov and Barnett, 1998a,b; McCabe et al. 2004; Hoerling et al. 2009; Herweijer et al. 2006; Kam et al. 2014; Steinman et al. 2012) and warm Atlantic conditions (Enfield et al. 2001; McCabe et al. 2008; Sutton and Hodson, 2005; Hodson et al. 2010) both exert strong controls on CONUS drought variability. Cold phases of the El-Niño Southern Oscillation (ENSO; La Niña events) and Pacific Decadal Oscillation (PDO) produce

atmospheric highs over the northern Pacific Ocean that shift subtropical jets poleward, divert storm tracks north, and cause precipitation deficits in the US Southwest and Great Plains in boreal winter (Sarachik and Cane, 2010; Trenberth and Guillemot, 1996; Ropelewski and Halpert 1986; Mantua et al. 1997; Seager et al. 2005; Hoerling et al. 2014). Warm phases of the AMO reduce summer precipitation broadly over the US by suppressing the Great Plains low-level jet and the North American Monsoon (Kushnir et al. 2010; Hu et al. 2011; Oglesby et al. 2012; Nigam et al. 2011; Williams et al. 2017). When these drought-favorable conditions occur simultaneously, the modes can collectively strengthen their hydroclimate influences over the CONUS (Mo et al. 2009; Hu and Feng 2012; Coats et al. 2015). For ENSO and PDO, which impose similar canonical wet-dry patterns over the CONUS (e.g., Baek et al. 2017), their combined hydroclimate influence is strengthened (weakened) when the two modes are in (out of) phase (Gershunov and Barnett, 1998a; Wang et al. 2014; Hu and Huang, 2009; Yu and Zwiers, 2007). AMO-induced drying over the Great Plains and Southeast, and to a lesser degree the Southwest can create a background state of persistent aridity or wetness over which influences from modes such as ENSO are imprinted. Given the above-described understanding, we hypothesize that a global ocean in which cold tropical Pacific and warm northern Atlantic conditions occur contemporaneously (Hoerling and Kumar 2003; McCabe et al. 2004, 2008) represent conditions that strongly increase the probability of pan-CONUS droughts (Schubert et al. 2009; Cook et al. 2014; Coats et al. 2015).

Studies that employ atmospheric general circulation models (AGCMs) forced with observed SSTs have not only reproduced these Pacific and Atlantic influences on drought over the CONUS (Schubert et al. 2004, 2008; Seager et al. 2005; Herweijer et al. 2006; Kushnir et al. 2010; Hoerling et al. 2009; Seager and Hoerling 2014), but have also emphasized the role of stochastic internal atmospheric variability in US hydroclimate (Seager

et al. 2014; Cook et al. 2018; Ault et al. 2017; Stevenson et al. 2015; Coats et al. 2015). Paleoclimate proxy-model comparisons demonstrate that coupled atmosphere-ocean GCMs reproduce the frequency and spatiotemporal characteristics of pan-CONUS droughts, but not due to the same underlying atmosphere-ocean states (e.g. Coats et al. 2015), thus further highlighting the influence of internal atmospheric variability on these events. Understanding differences between how pan-CONUS droughts are simulated and how they have occurred in the past is therefore critical for accurately characterizing future risks from these events.

Given the roles played by both the atmosphere and ocean, it is important to diagnose the relative contributions of the Pacific, Atlantic, and internal atmospheric variability to pan-CONUS droughts. Experiments that force AGCMs with global SSTs or regionally restricted SSTs represent one method of parsing these influences. For instance, Seager et al. (2005) examined 16-member ensembles from the NCAR Community Climate Model version 3 (CCM3) AGCM (Kiehl et al. 1998) forced with historical SSTs prescribed over (i) the global ocean or (ii) only over the tropical Pacific with a coupled ocean mixed layer elsewhere. These experiments demonstrated the primary role of tropical Pacific variability in forcing persistent droughts over the US Southwest and Great Plains. Similarly, Kushnir et al. (2010) used 16-member ensembles of the CCM3 AGCM forced with historical SSTs prescribed over (i) the global ocean or (ii) only over the tropical Atlantic with climatological SSTs elsewhere. They showed that warm tropical Atlantic conditions during April to September induce a Gill-type response that places a low to the west with northerly, subsiding flow over southwest North America, while warm tropical Atlantic conditions during October to March suppress convection over the tropical Pacific and create a La Niña-like atmospheric wave train. Their experiments thus supported a causal link between warm tropical Atlantic conditions and reduced precipitation over the US in both warm and cold seasons. In this paper, we use the three 16-member ensembles from Seager et al. (2005) and Kushnir et al. (2010) and an

additional 16-member ensemble from the newer Community Atmosphere Model version 5 (CAM5) AGCM forced with historical SSTs over the global ocean. These runs allow us to parse the contributions of ocean forcings and atmospheric variability to pan-CONUS droughts and compare model results to observations. Collectively, we address the following questions:

1) What are the respective roles of the tropical Pacific, Atlantic, and internal atmospheric variability in forcing pan-CONUS droughts?

2) What atmospheric and oceanic conditions are optimal for forcing pan-CONUS droughts?

3) Are identified atmospheric and oceanic conditions consistent across model simulations and observations?

2. Data and Methods

2.1. Model Data

We employ three 16-member ensembles of the CCM3 AGCM forced by three different prescribed oceanic conditions from 1856 to 2007 or 2012, depending on the experiment. SSTs are fixed in the following configurations: (i) Global Ocean-Global Atmosphere (GOGA), (ii) Pacific Ocean-Global Atmosphere-Mixed Layer (POGA-ML), and (iii) Tropical Atlantic-Global Atmosphere (TAGA). The GOGA configurations span 1856 − 2012 and force CCM3 with globally observed SSTs derived from Kaplan et al. (1998) and Hadley Centre Sea Ice and SST (HadISST; Rayner et al. 2003); Kaplan SST and HadISST were specified over the tropical Pacific (20°N − 20°S) from 1856 − 2012 and outside the tropical Pacific from 1870 − 2012, respectively. Kaplan SSTs were used if available outside the tropical Pacific from 1856 − 1870; climatological SSTs from HadISST were used otherwise (Seager et al. 2005). The POGA-ML configuration spans 1856 − 2012 and forces

CCM3 with a tropical Pacific specified with Kaplan SSTs, but otherwise couples the AGCM to a uniform mixed layer to calculate SSTs elsewhere (Seager et al. 2005). Finally, the TAGA configuration spans 1856 – 2007 and forces CCM3 with observed tropical Atlantic (30°N – 30°S) SSTs from the GOGA configuration but imposes climatological SSTs elsewhere (Kushnir et al. 2010). We also employ a 16-member ensemble from CAM5 that spans 1856 – 2016 and is forced with the same observed global SSTs used in the CCM3 GOGA experiment; we use only the 1856 – 2012 interval from this experiment for consistency with the CCM3 GOGA and POGA-ML experiments. For all of the model experiments, the ensemble mean is interpreted as the atmospheric state that is forced by the prescribed SSTs. While the sampled ensemble mean will always be influenced by random atmospheric noise, the effect will diminish as the size of the ensemble increases. To determine the robustness of the 16-member ensemble mean we have performed subsampling experiments with smaller ensemble sizes. Even a randomly selected 8-member ensemble generates a mean that is very similar to the ensemble mean using all 16 members (not shown). We therefore regard the ensemble mean from the 16 members as a robust characterization of the ocean forced response in the atmospheric model (Seager et al. 2005; Kushnir et al. 2010; Yang et al. 2017).

Volumetric soil moisture and geopotential height are taken from each simulation at 80-cm depth (linearly interpolated for CAM5) and 500-mbar height (501.3-mbar for TAGA), respectively. For the purposes of our analyses, these variables are standardized by subtracting and dividing by their respective 1856 – 2012 (2007 for TAGA) means and standard deviations. Analyzed SSTs are centered by subtracting their respective 1856 – 2012 (2007 for TAGA) means. We take June-July-August (JJA) averages for volumetric soil moisture and calendar-year averages for SST and geopotential height; JJA and December-January-February (DJF) averages are also taken for SST and geopotential height, but because our results do not change appreciably between DJF, JJA, and calendar-year averages, we only

show SST and geopotential height results for calendar-year averages. All fields are linearly detrended from 1856 – 2012 (2007 for TAGA) to remove the largest influences from anthropogenic warming effects and focus primarily on interannual to decadal signals. Output for all analyzed variables across all the ensembles have ~2.8° grid resolution.

2.2. Observational Data

We use monthly Model Calibrated Drought Index (MCDI) data from Williams et al. (2017) as our metric of JJA soil moisture over the observational record for comparison with the modeled soil moisture. MCDI covers the CONUS domain with 1/8° resolution from 1895 – present and is based on the Palmer Z-index, which is a standardized monthly formulation of a bucket soil moisture model forced by precipitation and reference evapotranspiration (Allen et al. 2005). By formulation, the Z-index contains little inter-monthly persistence of previous soil moisture conditions (Palmer 1965). In most other applications, the Z-index is used to calculate the Palmer Drought Severity Index (PDSI), but inter-month persistence of PDSI anomalies is prescribed based on field measurements from just one region of the CONUS (Palmer 1965). For the MCDI, inter-month persistence is spatially explicit, varies seasonally, and is calibrated to match that of monthly 0-200 cm soil-moisture anomalies simulated by the Noah Multi-Parameterization Land Surface Model (Ek et al., 2003; Niu et al., 2011), which includes effects of land-surface characteristics such as soil type and vegetation (Williams et al. 2017). The 0 – 200 cm depth is not only relevant for most root-zones, but also comparable to the 80-cm soil depth that is used from the models.

We employ the HadISST dataset and NOAA ESRL 20th Century Reanalysis Project Version 2c for monthly values of observational SST and reanalyzed geopotential height, respectively. HadISST has global SST coverage from 1870 to present on a 1° grid, while the 20th Century Reanalysis product offers, among several fields, global geopotential height coverage at 500 mbar from 1851 – 2014 on a 2° grid. We compute DJF, JJA, and calendar-

year means of SST and geopotential height from the observational products. In keeping with the model analyses, all MCDI, SST, and geopotential height fields are linearly detrended over their common interval from $1895 - 2014$. Again, because the results do not change appreciably between DJF, JJA, and calendar-year averages for SSTs and geopotential heights, we only show results for calendar-year averages.

2.3 Climate Indices

We use the NINO3.4 and AMO indices as characterizations of tropical Pacific and Atlantic Ocean variability, respectively. The NINO3.4 index is defined as linearly detrended DJF average SST anomalies in the $5°N - 5°S$ and $170° - 120°W$ region; El Niño and La Niña events are defined as years (concurrent with the year in which January and February are sampled) in which the NINO3.4 index is a half standard deviation above or below the mean, respectively. The AMO index is computed as the linearly detrended JJA average SST anomaly in the $0° - 60°N$ and $0° - 80°W$ region, with positive and negative AMO defined as years in which the AMO index is a half standard deviation above or below the mean, respectively.

2.4 Pan-CONUS Drought Analysis

We focus on a region of North America approximately encompassing the contiguous United States ($24.5 - 49°N$ to $59.5 - 127°W$), with some extension into northern Mexico. Pan-CONUS droughts are defined as years in which at least 50% of the area-weighted landmass of our study region is under drought, with drought classified at each grid point as when simulated JJA volumetric soil moisture at 80-cm depth is at least half a standard deviation below the mean. Our classification method thus treats pan-CONUS droughts as binary events (i.e. either a given year meets the pan-CONUS drought threshold or it does not). Our method furthermore counts the number of years of drought as opposed to the number of discrete drought events, even though some droughts span consecutive years. We

note that previous studies examining similarly widespread droughts over North America (e.g. Cook et al. 2014; Coats et al. 2015) have used a different definition of pan-CONUS droughts that require the area-averages of PDSI in at least three of four geographic regions (American Southwest, Central Plains, Southeast, and Northwest) to be simultaneously below a specific drought threshold. We have broken from this precedent to allow every location within the CONUS to potentially contribute to a pan-CONUS drought and to allow a more continuous measure of drought extent relative to a discrete measure defined by four specific regions. Both definitions nonetheless generate a similar selection of pan-CONUS droughts (not shown).

Using our definition, we composite (i) soil moisture, (ii) SST, and (iii) geopotential height for all pan-CONUS drought years across each 16-member ensemble:

$$X_C = \frac{\sum_{i=1}^{16} \sum_{j=1}^{N_i} X_{i,j}}{\sum_{i=1}^{16} N_i} = pan\text{-}CONUS\ Composite,$$

where $X_{i,j}$ is latitude-longitude matrix of either soil moisture, SST, or geopotential height in the ith ensemble member in a year, j, identified as a pan-CONUS drought year and N_i is the total number of pan-CONUS drought years in the ith ensemble. To isolate the component of the pan-CONUS drought composite forced by SSTs, we compute the 16-member ensemble mean, replicate it 16 times, and then composite across the same years identified as pan-CONUS droughts in each of individual ensemble members. We regard this later composite as the product of ocean forcing (e.g. Seager et al. 2005; Kushnir et al. 2010; Yang et al. 2017) and herein refer to it as the "ocean contribution" to pan-CONUS droughts:

$$X_O = \frac{\sum_{i=1}^{16} \sum_{j=1}^{N_i} \overline{X_{i,j}}}{\sum_{i=1}^{16} N_i} = Ocean\ Contribution,$$

where $\overline{X_{i,j}}$ is a latitude-longitude matrix of either soil moisture, geopotential height, or SST representing the ensemble average in year j of the ith ensemble member identified as a pan-CONUS drought year. The difference between the pan-CONUS drought composite and the

ocean contribution in any given ensemble year is attributed to internal atmospheric variability and referred to herein as the "atmospheric variability contribution:"

$$X_A = X_C - X_O = Atmospheric\ Variability\ Contribution$$

As a measure of the relative contributions to the pan-CONUS drought composite, we divide the volumetric soil moisture over the CONUS domain associated with the ocean contribution ($X_{O,SM}$) or atmospheric variability contribution ($X_{A,SM}$) by that of the total pan-CONUS drought composite ($X_{C,SM}$) (herein termed the "percent contribution" to the pan-CONUS drought).

$$\%\ Ocean\ Contribution = \frac{X_{O,SM}}{X_{C,SM}}$$

$$\%\ Atmospheric\ Varibility\ Contribution = \frac{X_{A,SM}}{X_{C,SM}}$$

Because we attribute all non-ocean forcings to atmospheric variability, our characterization of atmospheric variability will include any effects from land-surface feedbacks. The characterized atmospheric variability component is therefore not exclusively associated with the atmosphere, but our convention is sufficient for our present purpose, which is to specifically separate ocean influences from the other atmospheric and land conditions that generate pan-CONUS droughts. The potential role of land-surface feedbacks in impacting pan-CONUS droughts is nonetheless discussed in Section 4.

Pan-CONUS droughts and their associated SSTs and geopotential heights are also composited using the observational data over the interval from 1895 – 2014. We use the same definition of pan-CONUS drought and require that 50% of the area-weighted CONUS domain have MCDI values at least half a standard deviation below the mean at each grid point. We note that the MCDI represents 0-200 cm soil moisture as opposed to the 80 cm layer that is analyzed in the SST-forced model runs. Because the observational record represents just one realization of atmospheric variability over the observational interval given

the observed SST state, we do not decompose the contributions of ocean forcing and atmospheric variability as we do in the model experiments. We nevertheless compare the spatial features of modeled and observational pan-CONUS drought composites, as well as their years of incidence and frequency of occurrence.

3. Results

3.1 Does the CCM3 Model Simulate Pan-CONUS Droughts?

The distribution of the number of pan-CONUS droughts simulated across the CCM3 ensemble members from 1895 – 2012 (a period chosen to be roughly consistent with the available observational data) is represented as a boxplot in Figure 1. The 16 members produce 7 to 16 pan-CONUS drought years, the upper distribution of which is comparable to the 16 pan-CONUS droughts identified in the observation-based MCDI record. The CCM3 model thus not only simulates the occurrence of pan-CONUS droughts, but also a range of events that includes the number that occurred in the observational record. Figure 1 also plots time series of the number of CCM3 GOGA ensemble members simulating pan-CONUS droughts each year from 1856 – 2012, as well as the occurrence of observed pan-CONUS droughts as identified in the MCDI from 1895 – 2012. The distribution of pan-CONUS droughts is expected to be forced in part by SSTs, but based on analyses presented subsequently, atmospheric variability plays a significant role in driving pan-CONUS droughts and introduces significant variability in their occurrence.

3.2 CCM3 Ocean and Internal Atmospheric Influences

Figure 2 maps the composites for all pan-CONUS droughts across the CCM3 GOGA, POGA-ML, and TAGA 16-member ensembles from 1856 – 2012 (2007 for TAGA), as well as the associated SST and geopotential height anomalies. The corresponding ocean and atmospheric variability contributions to pan-CONUS droughts are also shown in Figure 2 for

each ensemble of simulations. The GOGA ensemble simulates 277 pan-CONUS droughts and yields a composite characterized by strong cooling over the tropical Pacific and strong warming over the northern Pacific, reflecting a clear La Niña and cold PDO pattern. Conversely, the Atlantic is characterized by largely neutral AMO conditions. Geopotential height anomalies at 500 mbar show a canonical La Niña-induced atmospheric ridge that stretches from the western north Pacific to eastern North America. These ocean contributions generally (Figure 2, middle column), and the La Niña conditions specifically, play a large role in the composited soil moisture anomalies during pan-CONUS droughts. Internal atmospheric variability (Figure 2, right column) nevertheless contributes a substantial additional ridge in this region centered over the US montane west. Ocean and internal atmospheric variability contribute a respective 53% and 47% to the severity of the simulated pan-CONUS droughts. Perhaps most importantly, atmospheric variability assists in drying specific regions of CONUS that appear to have weaker connections to ocean forcing. In the CCM3 GOGA ensemble, atmospheric variability assists drying in the montane West and the northeastern regions of CONUS, which are regions that dry less appreciably due to the associated ocean forcings.

The middle row of Figure 2 shows the composites for all pan-CONUS droughts in the 16-member CCM3 POGA-ML ensembles from 1856 − 2012. The POGA-ML ensemble experiment yields 248 pan-CONUS droughts, a small reduction from the 277 years simulated in the GOGA ensemble, and a pan-CONUS drought composite very similar to the GOGA experiment. Almost all associated SST and geopotential height anomalies associated with pan-CONUS droughts in the GOGA composite are preserved in the POGA-ML composite, albeit with anomalies that are more modest in magnitude. Although both the GOGA and POGA-ML ensembles have the same prescribed SSTs over the tropical Pacific, our selection of pan-CONUS droughts is selected only based on the criteria outlined in Section 2.4. The

high degree of similarity between the SST and geopotential height fields in the GOGA and POGA-ML ensembles are thus emergent characteristics underlying a common physical cause. Though less severe, the ocean and atmospheric variability contributions in the POGA-ML experiment are almost identical to their respective CCM3 GOGA counterparts in spatial extent; the SST and geopotential height fields in the GOGA and POGA-ML composite yields a spatial correlation of 0.62 and 0.94, respectively. Moreover, the ocean and atmospheric variability contribute a respective 46% and 54% to the severity of pan-CONUS droughts in the POGA-ML experiment, similar to the 53% and 47% contributions in the GOGA experiment. The high degree of similarity between the CCM3 GOGA and POGA-ML results not only highlights the importance of a cold tropical Pacific in driving pan-CONUS droughts, but also suggests that tropical Pacific variability accounts for virtually all the ocean forcing of pan-CONUS droughts in the GOGA simulations.

The TAGA ensemble experiment (Figure 2, bottom row) yields 189 pan-CONUS droughts, which is lower than the number simulated in the GOGA (N = 277) and POGA-ML (N = 248) experiments. This decrease is largely attributable to the greatly diminished contribution from ocean forcing as evidenced by a largely neutral tropical Atlantic with little to no SST anomalies associated with the pan-CONUS drought composite. The ocean contributes just 15% to the severity of pan-CONUS droughts and is tied to a uniformly modest drying over the CONUS domain. Conversely, atmospheric variability contributes 85% to the severity of the TAGA-simulated pan-CONUS droughts. The strong similarity between the pan-CONUS drought composite and the contribution from atmospheric variability is a clear indication that the atmosphere drives pan-CONUS droughts in the TAGA ensemble. Virtually all the atmospheric anomalies, particularly the CONUS ridge centered over the western CONUS, and all drying over CONUS are attributable to atmospheric variability in the TAGA experiment. The weak Atlantic Ocean contribution in

the TAGA experiment is consistent with what is inferred by the striking similarity of the POGA-ML and GOGA results. Given that the POGA-ML configuration only prescribes SSTs over the tropical Pacific and otherwise couples the AGCM to a uniform ocean mixed layer, Atlantic SSTs in the POGA-ML ensemble represent a teleconnected response to tropical Pacific forcings. The virtually identical Atlantic SSTs in the POGA-ML and GOGA results thus indicate that any role the Atlantic plays in forcing pan-CONUS droughts may themselves be a component of the tropical Pacific forcing. Within the CCM3 model, the very weak ocean contribution of the TAGA ensemble suggests that the Atlantic plays a limited role in driving pan-CONUS droughts and thus reinforces the dominant role of the tropical Pacific in forcing such events.

To further demonstrate the roles of the Pacific and Atlantic as characterized in the ensemble of simulations, we plot the NINO3.4 index in Figure 3 and the number of ensemble members simulating a pan-CONUS drought each year from 1856 – 2012 for both the GOGA and POGA-ML configurations. The occurrence of pan-CONUS drought years is not broadly synchronous across the two experiments, which is expected given that atmospheric variability contributes roughly half to the severity (and therefore occurrence) of pan-CONUS droughts in both experimental ensembles. There are furthermore no years in which all 16 members simulate pan-CONUS droughts, regardless of the ocean conditions; this is further in keeping with the large contribution from atmospheric variability, which can considerably obscure the oceanic forcings. Despite the influence of internal atmospheric variability, however, there are clear clusters of simulated pan-CONUS droughts during or very close to persistent La Niña years. For instance, 1857 – 1863, 1870 – 1876, 1893 – 1895, 1909 – 1911, 1945 – 1957, 1960 – 1963, 1974 – 1976, and 1999 – 2002 are all periods of high pan-CONUS drought occurrence across the 16-member ensembles that also fall during or otherwise span periods with multiple La Niña events. The dominant role of ENSO within the ocean forcing

component is also reflected in the mean NINO3.4 index across all pan-CONUS droughts, which is -0.47°C and -0.49°C for GOGA and POGA-ML, respectively. Similar to the Pacific analysis, Figure 4 plots a time series of the AMO index and the number of ensemble members simulating pan-CONUS droughts each year from 1856 – 2007 for the CCM3 GOGA and TAGA experiments. While there are clusters of pan-CONUS droughts (due to La Niñas) in the GOGA ensemble, the TAGA time series is more uniform, i.e. more randomly distributed across the ensemble. This is consistent with the dominant role played by atmospheric variability in the TAGA experiment. Furthermore, there does not appear to be any association between a given AMO state and pan-CONUS drought incidence in either the GOGA or TAGA ensembles. The mean AMO state during all pan-CONUS droughts is 0.0°C for both GOGA and TAGA ensembles. The potential role of the Atlantic is revisited in Section 3.5 in a combined observational and model analysis.

3.3 Atmospheric Variability: Hemispheric Patterns

The internal atmospheric variability contribution in the pan-CONUS drought composites consists of a high-pressure ridge over North America. The individual events represented within the composites, however, are generated by many dynamical patterns that do not distribute consistently in space. To illustrate this point, Figure 5 plots geopotential height anomalies due to atmospheric variability for eight individual pan-CONUS droughts from the CCM3 GOGA ensemble, as well as the global CCM3 GOGA composite for geopotential height and soil moisture across all pan-CONUS droughts. The oceanic influences have been removed from the geopotential height fields in Figure 5 to isolate the impacts of internal atmospheric variability. While the contribution of atmospheric variability to pan-CONUS droughts yields an atmospheric ridge over North America that is not connected to a wider hemispheric pressure pattern, Figure 5 shows eight unique events with considerable range in their hemispheric pressure patterns. Any given year could have

conditions that deviate from the composite pattern so long as the net influence of the ocean and atmospheric variability forces a ridge, and thus drying, over North America.

3.4 Comparison of CCM3 and CAM5 GOGA Simulations

The CCM3 has been shown to simulate precipitation variability over the CONUS domain with excellent fidelity (e.g. Seager et al. 2005; Seager and Hoerling, 2014; Hack et al. 1998), but it is an older generation atmospheric model. We therefore compare the simulation of pan-CONUS droughts in the CCM3 GOGA ensemble to a 16-member GOGA ensemble generated with the newer CAM5. Figure 6 shows the composite for all pan-CONUS droughts across the CAM5 GOGA ensemble with its associated SST and geopotential height anomalies, as well as its corresponding ocean and atmospheric variability contributions to pan-CONUS droughts. The CAM5 and CCM3 GOGA composites simulate similar numbers of pan-CONUS droughts over the full 16-member ensembles: 303 and 277, respectively, and exhibit broad consistencies in their spatial features (i.e. between the top row of Figure 2 and Figure 6). This provides support for interpretations of the CCM3 simulations as representative of responses in newer-generation models. There nonetheless are some differences between the CCM3 and CAM5 simulations. For instance, CCM3 associates larger SST anomalies with pan-CONUS droughts in the Pacific, as well as a stronger atmospheric response to those SSTs. In contrast, CAM5 associates pan-CONUS droughts with more modest SST anomalies globally, which is reflected in the CAM5 ocean contribution (39%) being less than that of CCM3 (53%). Pan-CONUS drought conditions thus appear more strongly dictated by SSTs in the CCM3 model than in the CAM5 model. Despite these differences, the results provide some confidence that the associations between pan-CONUS droughts, ocean forcings, and atmospheric variability are consistent across the two generations of models, even though we do not currently have CAM5 simulations with POGA-ML and TAGA configurations to fully test the consistency. The agreement across the

GOGA ensembles and the demonstrated skill of CCM3 in simulations of North American hydroclimate is nevertheless suggestive of the fact that the analyzed behavior of CCM3 is not a unique feature of the earlier generation of NCAR model.

3.5 ENSO and AMO Influence on the Spatial Extent of CONUS Droughts

We use both the CCM3 and CAM5 GOGA ensembles to generate boxplots for the percent of CONUS under drought (determined by dividing the number of grid points under drought by the total number of grid points) from 1856 − 2012 under various conditions (Figure 7). The "All" column is a boxplot of the percent of CONUS under drought for all years. The "NINO3.4 < -1.5," "-1.5 < NINO3.4 < -1.0," and " -1.0 < NINO3.4 < -0.5" columns show GOGA ensemble aggregate boxplots of the percent of CONUS under drought only for years in which the NINO3.4 index is < -1.5, -1.5 to -1.0, and -1.0 to -0.5 standard deviations from the mean, respectively. Similarly, the "AMO > 1.0" and "AMO < -1.0" columns provide boxplots of the percent of CONUS under drought only for years in which the AMO index is greater than one standard deviation above and less than one standard deviation below the mean, respectively, in the two GOGA simulations. These variously sampled distributions indicate that La Niñas increase the percent of CONUS under drought in both the CCM3 and CAM5 experiments. As the severities of La Niña events intensify, the percent of CONUS under drought also generally increases. In contrast, the percent of CONUS under drought decreases (very slightly for the CCM3) for the subset of years in which the AMO index is one standard deviation above the mean, which is opposite of the expected response (e.g. Kushnir et al. 2010). The percent of CONUS under drought also decreases for the subset of years in which the AMO index is one standard deviation below the mean.

The distributions of the various samples above are tested for significance using a two-way Kolmogorov–Smirnov (KS) test (Chakravarti et al. 1967). The percent of CONUS under

drought during La Niñas increases significantly (p<0.05) relative to the distribution that includes all years in both the CCM3 and CAM5 GOGA experiments; this is true for all subsets of La Niña extremeness. The percent of CONUS under drought during warm AMO events (AMO > 1.0 standard deviation), is significantly smaller (p<0.05) than the distribution that includes all years for the CAM5 experiment, while the CCM3 experiment is not significantly different from the distribution for all years. The percent of CONUS under drought during cold AMO events (AMO < -1.0 standard deviation) is significantly smaller (p<0.05) than the distribution that includes all years for both the CCM3 and CAM5 experiment. The percent of CONUS under drought during warm AMO events is significantly different from that during cold AMO events for CCM3, while the difference is not significant for CAM5. For the subset of years in which the AMO index is more than half a standard deviation above or below the mean, neither the CAM5 nor the CCM3 experiments yield distributions that are significantly different from the distribution that includes all years. At the half standard deviation threshold, the percent of CONUS under drought during warm AMO events is moreover not significantly different from that during cold AMO events for both the CCM3 and CAM5. Our significance tests show cold Pacific conditions to clearly impact the percent of US under drought but yield results that are not significant for warm Atlantic conditions; the only significant result is for CAM5, but towards a wetting instead of drying. While reasonably instructive in the context of the GOGA experiments, we also note that these assessments may combine ENSO and AMO influences and thus are not as definitive as the other analyses we have performed herein to separate the Pacific and Atlantic influences.

3.6 Sensitivity of results to pan-CONUS drought definition

A threshold of 50% of the study area is used to define pan-CONUS droughts throughout the model analyses. Here we explore the sensitivity of our results to higher spatial thresholds. Table 1 shows the number of pan-CONUS droughts, the percent ocean

contribution, and the percent atmospheric variability contribution for spatial thresholds of 50%, 55%, 60%, 65%, and 70% area for each of the four 16-member ensembles. The number of pan-CONUS droughts predictably decreases across all four ensembles as the spatial extent criterion increases. The decreases are substantial—each 5% increase in area cuts the number of pan-CONUS droughts by as much as 50%, demonstrating that the number of pan-CONUS droughts is sensitive to the value of the spatial threshold. The relative contributions of the ocean and atmospheric variability are nonetheless robust across the range of spatial thresholds, notwithstanding increasingly higher contributions from atmospheric variability for larger spatial thresholds. This increase is consistent with the results of Figure 2 that show atmospheric variability to play a key role in drying regions of CONUS with weaker connections to ocean forcings. Given that ocean-induced drying may be spatially limited to regions of strong teleconnections, it is perhaps expected that the contribution of atmospheric variability to pan-CONUS droughts must increase with higher spatial thresholds. The trend toward higher atmospheric variability contributions with increased drought-area thresholds is evident in the CAM5 GOGA, CCM3 GOGA, and CCM3 POGA-ML ensembles, but nonexistent in the CCM3 TAGA ensemble, as essentially all droughts were driven by atmospheric variability in that experiment.

3.7 Comparison to Observations

The top panel of Figure 8 shows a composite of mean observed MCDI, geopotential height, and SST anomalies during observed pan-CONUS drought years (N = 16) from 1895 – 2014. There is evidence of weak La Niña-like conditions in the tropical Pacific, but the northern Pacific is reflective of a warm PDO pattern, as opposed to the cold PDO pattern that emerges in the models. The atmospheric ridge does not resemble a canonical La Niña-forced response but is more like the atmospheric contribution plots of Figure 2, likely attesting to the fact that the observed ridge is caused mainly by internal atmospheric variability. Furthermore,

Figure 8 shows a warm north Atlantic basin that forms a canonical positive AMO horseshoe pattern over the North Atlantic in observed pan-CONUS drought years, which is not seen in our model results. Interpretations of differences between the observational and model results, however, must consider the limited sample size of 16 observed pan-CONUS droughts relative to the increased sampling provided by the 16-member model ensembles and the dominant role of internal atmospheric variability inferred from the models. These considerations are particularly important for the Atlantic given its possibly stronger role over decadal to centennial timescales (as opposed to the incidence of yearly events that we have analyzed in the context of pan-CONUS droughts), which makes even more ambiguous the association between the Atlantic warm anomaly and pan-CONUS droughts suggested by Figure 8 (this is similarly true of the contrasting PDO states in the observations and model simulations).

With the above perspective, we further sub-composite the 16 observed pan-CONUS drought years based on the value of their associated AMO index. The distribution of the AMO index for the 16 pan-CONUS droughts (Figure 9, bottom) yields three cold AMO, seven neutral AMO, and six warm AMO years thereby suggesting that the pan-CONUS drought composite (Figure 8, top) is weighted towards warm Atlantic conditions by just six of the 16 years. The cold and neutral AMO groups furthermore include La Niña conditions, pointing to conflated Pacific and Atlantic hydroclimatic influences. While the strong AMO group indicates weak El Niño conditions, the significance of the six years is ambiguous when considering that there are 42 years in which the AMO index is at least half a standard deviation above its 1895 – 2012 interval mean. In other words, it is entirely possible that the warm AMO association seen in the composite over the observational record is due to chance.

To further demonstrate this possibility, we subsample from the two GOGA ensembles the same 16 years in which pan-CONUS droughts occurred in the observational data, yielding 256 model years for each of the CCM3 and CAM5 16-member experiments. Some of these

256 model years will have pan-CONUS droughts and others will not; Figure 9 shows the composites for (i) those years that yield pan-CONUS droughts and (ii) those years that do not. We note that SSTs from the GOGA simulations and HadISST are both observation-based and nearly identical; while there is potential for model biases in the atmospheric response (e.g. Merrifield and Xie, 2016), there are no such biases in the GOGA SST fields. Figure 9 thus provides a very close approximation of how the same SSTs seen in the observational composite (Figure 9) contribute to droughts in the models. If the Atlantic were at play, we would expect an increased incidence of pan-CONUS droughts relative to the rate over all years (1856 – 2012) of the 16-member GOGA ensembles. However, only 10.9 – 12.9% of the 256 selected model years (28/256 and 33/256 for the CAM5 and CCM3 GOGA experiments, respectively) simulate pan-CONUS droughts, which is comparable to the frequency of pan-CONUS drought simulated in all years from the GOGA runs (12.1% and 11.0% for CAM5 and CCM3, respectively). Warm Atlantic conditions thus do not seem to affect the likelihood of pan-CONUS droughts in the model simulations and even the 28 to 33 pan-CONUS drought years that include warm AMO conditions are accompanied in aggregate by conflated warm extratropical North Atlantic and strong La Niña conditions, making it highly ambiguous whether warm Atlantic conditions contributed to pan-CONUS conditions in any material way. Additionally, the warm SSTs in the North Atlantic do not extend into the tropics where the principle association with North American hydroclimate resides (Sutton and Hodson 2005, 2007, Kushnir et al. 2010; Ruprich-Robert, 2017) and the composite of years that do not simulate pan-CONUS droughts yield neutral hydroclimate conditions over the CONUS in both the CAM5 and CCM3 ensembles despite anomalously warm northern Atlantic conditions. Conversely, the same composite shows a tropical Pacific with largely neutral to only very weak La Niña conditions.

These results highlight an advantage of the combined GOGA, POGA-ML, and TAGA model experiments, namely their ability to isolate Pacific and Atlantic influences. More importantly, they demonstrate that associations between the Atlantic and pan-CONUS droughts in the observations and model simulations are likely not at odds, but rather reconcilable when considering the limited sampling and likely conflation of Pacific and Atlantic influences in the observational data.

4. Discussion and Conclusions

This study has assessed the contributions of ocean forcing and atmospheric variability to pan-CONUS droughts using atmospheric model experiments forced with multiple configurations of global or regional SSTs. Our analysis of simulated pan-CONUS droughts demonstrates that internal atmospheric variability plays a role that is roughly equal to or greater than the collective ocean forcing; internal atmospheric variability can combine with the ocean forcing to either nullify or amplify drying. Tropical Pacific Ocean variability alone can explain virtually all of the ocean contribution to pan-CONUS droughts. Conversely, the model results suggest that the Atlantic does not play a significant role in forcing pan-CONUS droughts, as there is little association between these droughts and warm conditions in the north Atlantic. While observations do appear to associate a warm Atlantic with pan-CONUS droughts, closer analyses suggest that this association is not robust given the small number of years that qualify as pan-CONUS drought events in the observational data (N = 16), the dominant role of atmospheric variability, and the conflated influences of the Atlantic and Pacific Oceans. The model results as they relate to the Atlantic are thus not necessarily at odds with observations, but the comparison is limited given the small sample size in the observational dataset.

Our results are notwithstanding the caveat that we have examined only a single lineage of atmospheric model, namely the NCAR CCM3 and CAM5 models, and a relatively coarse resolution for each. The associations we have characterized in this study may therefore not extend across multiple models when considering varying model biases, model resolutions, and model responses to similar forcings. Additional experiments using different models and resolutions are thus important for determining whether the associations that we have characterized are specific to CCM3 and CAM5. One limitation is that there are few SST-forced model ensembles of comparable size and length to the 16-member ensembles we have analyzed herein. Many existing forced-SST modeling experiments employ ensembles that are on the order of only 3-5 members and only cover the post-1979 period (e.g. the AMIP CMIP5 experiments; Taylor et al. 2012), a reality that is not likely to change in CMIP6 (Eyring et al. 2016). A multi-model ensemble analysis is nevertheless needed to assess whether the model characterization that we present herein is consistent across many models, and most importantly whether it is consistent with reality.

Nonetheless, the large role of internal atmospheric variability found in our results has key implications for the predictability of pan-CONUS droughts. Although statistical and physical models can predict El Niños and La Niñas with varying skill six or (sometimes) more months in advance (Latif et al. 1994, 1998; Cane et al. 1986; Graham et al. 1987a,b; Barnett et al. 1988; Barnston and Ropeleski, 1992; Barnston et al. 2012), predicting internal atmospheric variability is limited to shorter lead times due to the chaos of atmospheric motions and the absence of guiding by slower evolving ocean conditions. According to our modeling results, internal atmospheric variability complicates the predictability of pan-CONUS droughts because it can either exacerbate or nullify drying imposed by La Niñas, leading to (i) strong La Niña years with low incidence of pan-CONUS droughts (1880, 1904, 1925, 1943, 1999, 2000, 2006, 2008, 2011), (ii) weak La Niña years with high incidence of

pan-CONUS droughts (1872, 1895, 1946, 1960, 1962, 1975), and even (iii) strong El Niño years with pan-CONUS droughts (1897, 1900, 1903, 1912, 1931, 1964, 1966, 1969, 1973, 1977, 2003). Despite the unequivocal influence of La Niñas, the ocean forcing contributes only ~50% to the severity of the pan-CONUS drought composite; the large role of atmospheric variability relative to the ocean forcing thus poses an inherent limit to the predictability of these events.

Though not considered in our study, we note the important role of land-surface feedbacks on the hydrological cycle over the US (Xue et al. 2001; Beljaars et al. 1996; Koster et al. 2003, 2009, 2012) and the potential for antecedent soil moisture conditions to influence the occurrence of pan-CONUS droughts. Antecedent soil moisture not only imposes a supply-side constraint on evapotranspiration that limits the amount of precipitation recycled back to a region (Elfatih et al. 1996; Wang-Erlandsson et al. 2014; Koster et al. 2009), but through its influence on latent cooling (Fisher et al. 2007a, b) and vegetation (Charney 1975, 1977), also modifies albedo, surface heat flux, planetary boundary layer height, and convective energy (Koster et al. 2011, 2014, 2016; Guo et al. 2011, Cook et al. 2015). Studies suggest a positive feedback between soil moisture and precipitation (wetter soils lead to more evapotranspiration leading to more precipitation and wetter soils) and have identified regions of CONUS as hotspots of soil moisture-precipitation coupling (Koster et al. 2004, 2006, 2016; Pal and Eltahir, 2002; Findell et al. 1997, 2003). Hence, properly modeling land-surface feedbacks over coupling hotspots may offer increased predictability of pan-CONUS droughts. In this study, the implications for predictive power of pan-CONUS droughts beyond the timescale of internal atmospheric predictability are limited to those regions of CONUS that are sensitive to ocean forcings (i.e. US Southwest and Central Plains). While we have attributed all non-ocean forced drying to atmospheric variability, it is likely that some of

this drying can be attributed to land-surface feedbacks, which would increase the potential predictability of pan-CONUS droughts.

Notwithstanding land-surface influences and the abovementioned caveat, our results suggest the contemporaneous cold Pacific Ocean and warm Atlantic Ocean identified as being ideal for drought over North America (Hoerling and Kumar 2003; Schubert et al. 2009) is unlikely to generate drought across enough of the US to cause a pan-CONUS drought when unaided by internal atmospheric variability. Moreover, we find little evidence for a strong Atlantic influence, in contrast to previous findings. For instance, Cook et al. (2014) and Coats et al. (2015) found negative correlations between the AMO and (i) tree-ring PDSI in the North American Drought Atlas and (ii) PDSI calculated in last-millennium simulations from the CMIP5/PIMP3 archive, respectively. Coats et al. (2015) furthermore concluded that pan-CONUS drought probabilities increase during warm phases of the AMO. We note, however, that both studies derived those associations with positive AMO conditions using observational data and are thus subject to the same possibility of conflated Pacific influences that were explored in Section 3.6. Our Atlantic results are also distinct from previous studies that show an active AMO influence on multi-decadal droughts (Cook et al. 2016; Feng et al. 2008, 2011; Coats et al. 2015, 2016). While single-year pan-CONUS events are strongly dependent on ENSO and atmospheric variability, decadal-scale events are associated with smaller hydroclimate anomalies and may be more sensitive to the slight but persistent background drying that the AMO can provide. Pan-CONUS droughts and multi-decadal droughts are thus not directly comparable, and our results should be interpreted with caution regarding AMO influences on droughts over multi-decadal timescales.

Acknowledgements

References

Allen, R. G., Walter, I. A., Elliot, R., Howell, T., Itenfisu, D., Jensen, M. (2005), The ASCE Standardized Reference Evapotranspiration Equation, *Rep. 978-0-7844-0805-X*, 59 pp, Task Committee on Standardization of Reference Evapotranspiration of the American Society of Civil Engineers, Reston, VA. http://www.kimberly.uidaho.edu/water/asceewri/.

Andreadis, K. M., Clark, E. A., Wood, A. W., Hamlet, A. F. & Lettenmaier, D. P. Twentieth-Century Drought in the Conterminous United States. *J. Hydrometeorol.* **6,** 985–1001 (2005).

Ault, T. R., George, S. S., Smerdon, J. E., Coats, S., Mankin, J. S., Carrillo, C. M., … Stevensong, S. (2018). A robust null hypothesis for the potential causes of megadrought in Western North America. *Journal of Climate*, *31*(1), 3–24. https://doi.org/10.1175/JCLI-D-17-0154.1

Baek, S. H., Smerdon, J. E., Coats, S., Williams, A. P., Cook, B. I., Cook, E. R., & Seager, R. (2017). Precipitation, temperature, and teleconnection signals across the combined North American, monsoon Asia, and old world drought atlases. *Journal of Climate*, *30*(18), 7141–7155. https://doi.org/10.1175/JCLI-D-16-0766.1

Barnett, T., Graham, N., Cane, M., Zebiak, S., Dolan, S., O'Brien, J., & Legler, D. (1988). On the Prediction of the El Nino of 1986-1987. *Science*, *241*(4862), 192–196. https://doi.org/10.1126/science.241.4862.192

Barnston, A. G., & Ropelewski, C. F. (1992). Prediction of ENSO episodes using canonical correlation analysis. *Journal of Climate*. https://doi.org/10.1175/1520-0442(1992)005<1316:POEEUC>2.0.CO;2

Barnston, A. G., Tippett, M. K., L'Heureux, M. L., Li, S., & Dewitt, D. G. (2012). Skill of real-time seasonal ENSO model predictions during 2002-11: Is our capability increasing? *Bulletin of the American Meteorological Society*, *93*(5), 631–651. https://doi.org/10.1175/BAMS-D-11-00111.1

Beljaars, A. C. M., Viterbo, P., Miller, M. J., & Betts, A. K. (1996). The Anomalous Rainfall over the United States during July 1993: Sensitivity to Land Surface Parameterization and Soil Moisture Anomalies. *Monthly Weather Review*. https://doi.org/10.1175/1520-0493(1996)124<0362:TAROTU>2.0.CO;2

Cane, M. A., Zebiak, S. E., & Dolan, S. C. (1986). Experimental forecasts of El Niño. *Nature*, *321*, 827. Retrieved from http://dx.doi.org/10.1038/321827a0

Charney, J. G. (1975). Dynamics of deserts and drought in the Sahel. *Quarterly Journal of the Royal Meteorological Society*, *101*(428), 193–202. https://doi.org/10.1002/qj.49710142802

Charney, J., Quirk, W. J., Chow, S., & Kornfield, J. (1977). A Comparative Study of the Effects of Albedo Change on Drought in Semi–Arid Regions. *Journal of the*

Atmospheric Sciences. https://doi.org/10.1175/1520-0469(1977)034<1366:ACSOTE>2.0.CO;2

Chakravarti, Laha, and Roy, (1967). Handbook of Methods of Applied Statistics, Volume I, John Wiley and Sons.

Coats, S., Smerdon, J. E., Cook, B. I., Seager, R., Cook, E. R., & Anchukaitis, K. J. (2016). Internal ocean-atmosphere variability drives megadroughts in Western North America. *Geophysical Research Letters*, *43*, 9886–9894. https://doi.org/10.1002/2016GL070105.Received

Coats, S., Cook, B. I., Smerdon, J. E., & Seager, R. (2015). North American Pancontinental Droughts in Model Simulations of the Last Millennium*. *Journal of Climate*, *28*(5), 2025–2043. https://doi.org/10.1175/JCLI-D-14-00634.1

Coats, S., Smerdon, J. E., Cook, B. I., & Seager, R. (2015). Are Simulated Megadroughts in the North American Southwest Forced ?*. *Journal of Climate*, *28*(1), 124–143. https://doi.org/10.1175/JCLI-D-14-00071.1

Cook, B. I., Cook, E. R., Smerdon, J. E., Seager, R., Williams, A. P., Coats, S., … Díaz, J. V. (2016). North American megadroughts in the Common Era: Reconstructions and simulations. *Wiley Interdisciplinary Reviews: Climate Change*, *7*(3), 411–432. https://doi.org/10.1002/wcc.394

Cook, B. I., Park Williams, A., Mankin, J. S., Seager, R., Smerdon, J. E., & Singh, D. (2018). Revisiting the leading drivers of Pacific coastal drought variability in the contiguous United States. *Journal of Climate*, *31*(1), 25–43. https://doi.org/10.1175/JCLI-D-17-0172.1

Cook, B. I., Shukla, S. P., Puma, M. J., & Nazarenko, L. S. (2015). Irrigation as an historical climate forcing. *Climate Dynamics*, *44*(5–6), 1715–1730. https://doi.org/10.1007/s00382-014-2204-7

Cook, B. I., Smerdon, J. E., Seager, R., & Cook, E. R. (2014). Pan-Continental Droughts in North America over the Last Millennium. *Journal of Climate*, *27*(1), 383–397. https://doi.org/10.1175/JCLI-D-13-00100.1

Ek, M. B., Mitchell, K. E., Lin, Y., Rogers, E., Grunmann, P., Koren, V., … Tarpley, J. D. (2003). Implementation of Noah land surface model advances in the National Centers for Environmental Prediction operational mesoscale Eta model. *Journal of Geophysical Research*, *108*(D22), 8851. https://doi.org/10.1029/2002JD003296

Elfatih, A., Elthahir, B., & Bras, R. L. (1996). Precipitation Recycling. *Reviews of Geophysics*, (96), 367–378. https://doi.org/10.1029/96RG01927

Enfield, D. B., Mestas-Nuñez, A. M., & Trimble, P. J. (2001). The Atlantic multidecadal oscillation and its relation to rainfall and river flows in the continental U.S. *Geophysical Research Letters*, *28*(10), 2077–2080. https://doi.org/10.1029/2000GL012745

Eyring, V. et al. Overview of the Coupled Model Intercomparison Project Phase 6 (CMIP6) experimental design and organization. *Geosci. Model Dev.* **9,** 1937–1958 (2016).

Feng, S., Hu, Q., & Oglesby, R. J. (2011). Influence of Atlantic sea surface temperatures on persistent drought in North America. *Climate Dynamics*, *37*(3), 569–586. https://doi.org/10.1007/s00382-010-0835-x

Feng, S., Oglesby, R. J., Rowe, C. M., Loope, D. B., & Hu, Q. (2008). Atlantic and Pacific SST influences of medieval drought in North America simulated by the Community Atmospheric Model. *Journal of Geophysical Research Atmospheres*, *113*(11), 1–14. https://doi.org/10.1029/2007JD009347

Findell, K. L., & Eltahir, E. A. B. (1997). An analysis of the soil moisture-rainfall feedback, based on direct observations from Illinois. *Water Resources Research*, *33*(4), 725–735. https://doi.org/10.1029/96wr03756

Findell, K. L., & Eltahir, E. A. B. (2003). Atmospheric Controls on Soil Moisture–Boundary Layer Interactions. Part II: Feedbacks within the Continental United States. *Journal of Hydrometeorology*, *4*(3), 570–583. https://doi.org/10.1175/1525-7541(2003)004<0570:ACOSML>2.0.CO;2

Fischer, E. M., Seneviratne, S. I., Vidale, P. L., Lüthi, D., & Schär, C. (2007). Soil moisture-atmosphere interactions during the 2003 European summer heat wave. *Journal of Climate*, *20*(20), 5081–5099. https://doi.org/10.1175/JCLI4288.1

Fischer, E. M., Seneviratne, S. I., Lüthi, D., & Schär, C. (2007). Contribution of land-atmosphere coupling to recent European summer heat waves. *Geophysical Research Letters*, *34*(6), 1–6. https://doi.org/10.1029/2006GL029068

Gershunov, A., & Barnett, T. P. (1998). Interdecadal modultion of ENSO teleconnections. *Bulletin of the American Meteorological Society*, *79*, 2715–2726. https://doi.org/10.1175/1520-0477(1998)079<2715:imoet>2.0.co;2

Gershunov, A., & Barnett, T. P. (1998). ENSO influence on intraseasonal extreme rainfall and temperature frequencies in the contiguous United States: Implications for long-range predictability. *Journal of Climate*, *11*(12), 3192–3203. https://doi.org/10.1175/1520-0442(1998)011<3192:EIOIER>2.0.CO;2

Graham, N. E., & Michaelsen, J. (1987). An Investigation of the El Niño-Southern Oscillation Cycle With Statistical Models 2. Model Results, *92*(7).

Graham, N. E., Michaelsen, J., & Barnett, T. P. (1987). An Investigation of the El Niño-Southern Oscillation Cycle With Statistical Models 1. Predictor Field Characteristics, *92*(7).

Guo, Z., Dirmeyer, P. A., & Delsole, T. (2011). Land surface impacts on subseasonal and seasonal predictability. *Geophysical Research Letters*, *38*(24), 1–5. https://doi.org/10.1029/2011GL049945

Hack, J. J., Kiehl, J. T., & Hurrell, J. W. (1998). The hydrologic and thermodynamic characteristics of the NCAR CCM3. *Journal of Climate*, *11*(6), 1179–1206. https://doi.org/10.1175/1520-0442(1998)011<1179:THATCO>2.0.CO;2

Herweijer, C., Seager, R., & Cook, E. R. (2006). North American droughts of the mid to late nineteenth century: a history, simulation and implication for Mediaeval drought. *Holocene*, *16*(2), 159–171. https://doi.org/10.1191/0959683606hl917rp

Hodson, D. L. R., Sutton, R. T., Cassou, C., Keenlyside, N., Okumura, Y., & Zhou, T. (2010). Climate impacts of recent multidecadal changes in Atlantic Ocean Sea Surface Temperature: A multimodel comparison. *Climate Dynamics*, *34*(7), 1041–1058. https://doi.org/10.1007/s00382-009-0571-2

Hoerling, M., Eischeid, J., Kumar, A., Leung, R., Mariotti, A., Mo, K., … Seager, R. (2014). Causes and predictability of the 2012 great plains drought. *Bulletin of the American Meteorological Society*. https://doi.org/10.1175/BAMS-D-13-00055.1

Hoerling, M., & Kumar, A. (2003). The perfect ocean for drought. *Science*, *299*(5607), 691–694. https://doi.org/10.1126/science.1079053

Hoerling, M., Quan, X. W., & Eischeidi, J. (2009). Distinct causes for two principal U.S. droughts of the 20th century. *Geophysical Research Letters*, *36*(19), 1–6. https://doi.org/10.1029/2009GL039860

Hu, Q., & Feng, S. (2012). AMO- and ENSO-driven summertime circulation and precipitation variations in North America. *Journal of Climate*, *25*(19), 6477–6495. https://doi.org/10.1175/JCLI-D-11-00520.1

Hu, Q., Feng, S., & Oglesby, R. J. (2011). Variations in North American summer precipitation driven by the Atlantic multidecadal oscillation. *Journal of Climate*, *24*(21), 5555–5570. https://doi.org/10.1175/2011JCLI4060.1

Hu, Z.-Z., & Huang, B. (2009). Interferential Impact of ENSO and PDO on Dry and Wet Conditions in the U.S. Great Plains, (1955), 6047–6065. https://doi.org/10.1175/2009JCLI2798.1

Kam, J., Sheffield, J., & Wood, E. F. (2014). Changes in drought risk over the contiguous UnitedStates (1901–2012): The influence of the Pacificand Atlantic Oceans. *Geophys. Res. Lett.*, *41*, 5897–5903. https://doi.org/10.1002/2014GL060973.Received

Kiehl, J. T., Hack, J. J., Bonan, G. B., Boville, B. A., Williamson, D. L., & Rasch, P. J. (1998). The National Center for Atmospheric Research Community Climate Model: CCM3. *Journal of Climate*, *11*(6), 1131–1149. https://doi.org/10.1175/1520-0442(1998)011<1131:TNCFAR>2.0.CO;2

Kogan, F. N. Droughts of the Late 1980s in the United States as Derived from NOAA Polar-Orbiting Satellite Data. *Bull. Am. Meteorol. Soc.* **76,** 655–668 (1995).

Koster, R. D., Guo, Z., Dirmeyer, P. a., Bonan, G. B., Chan, E., Cox, P. M., … Yamada, T. (2006). GLACE: The Global Land – Atmosphere Coupling Experiment. Part I:

Overview. *Journal of Hydrometeorology*, *7*, 611–625.
https://doi.org/http://dx.doi.org/10.1175/JHM511.1

Koster, R. D., Mahanama, S. P. P., Yamada, T. J., Balsamo, G., Berg, A. A., Boisserie, M.,
… Wood, E. F. (2011). The Second Phase of the Global Land–Atmosphere Coupling
Experiment: Soil Moisture Contributions to Subseasonal Forecast Skill. *Journal of
Hydrometeorology*, *12*(5), 805–822. https://doi.org/10.1175/2011JHM1365.1

Koster, R. D., Guo, Z., Bonan, G., Chan, E., & Cox, P. (2004). Regions of Strong Coupling
Between Soil Moisture and Precipitation. *Science*, *1138*(2004), 10–13.
https://doi.org/10.1126/science.1100217

Koster, R. D., Chang, Y., & Schubert, S. D. (2014). A mechanism for land-atmosphere
feedback involving planetary wave structures. *Journal of Climate*, *27*(24), 9290–9301.
https://doi.org/10.1175/JCLI-D-14-00315.1

Koster, R. D., Chang, Y., Wang, H., & Schubert, S. D. (2016). Impacts of local soil moisture
anomalies on the atmospheric circulation and on remote surface meteorological fields
during boreal summer: A comprehensive analysis over North America. *Journal of
Climate*, *29*(20), 7345–7364. https://doi.org/10.1175/JCLI-D-16-0192.1

Koster, R. D., Guo, Z., Yang, R., Dirmeyer, P. A., Mitchell, K., & Puma, M. J. (2009). On
the nature of soil moisture in land surface models. *Journal of Climate*, *22*(16), 4322–
4335. https://doi.org/10.1175/2009JCLI2832.1

Koster, R. D., & P. Mahanama, S. P. (2012). Land Surface Controls on Hydroclimatic Means
and Variability. *Journal of Hydrometeorology*, *13*(5), 1604–1620.
https://doi.org/10.1175/JHM-D-12-050.1

Koster, R. D., Suarez, M. J., Higgins, R. W., & Van den Dool, H. M. (2003). Observational
evidence that soil moisture variations affect precipitation. *Geophysical Research Letters*,
30(5), n/a-n/a. https://doi.org/10.1029/2002GL016571

Koster, R. D., Schubert, S. D., & Suarez, M. J. (2009). Analyzing the concurrence of
meteorological droughts and warm periods, with implications for the determination of
evaporative regime. *Journal of Climate*, *22*(12), 3331–3341.
https://doi.org/10.1175/2008JCLI2718.1

Kushnir, Y., Seager, R., Ting, M., Naik, N., & Nakamura, J. (2010). Mechanisms of tropical
atlantic SST influence on North American precipitation variability. *Journal of Climate*,
23(21), 5610–5628. https://doi.org/10.1175/2010JCLI3172.1

Latif, M., Anderson, D., Barnett, T., Cane, M., Kleeman, R., Leetmaa, A., … Schneider, E.
(1998). A review of the predictability and prediction of ENSO. *Journal of Geophysical
Research: Oceans*, *103*(C7), 14375–14393. https://doi.org/10.1029/97JC03413

Latif, M., Barnett, T. P., Cane, M. A., Flügel, M., Graham, N. E., von Storch, H., … Zebiak,
S. E. (1994). A review of ENSO prediction studies. *Climate Dynamics*, *9*(4–5), 167–
179. https://doi.org/10.1007/BF00208250

Mantua, N. J., Hare, S. R., Zhang, Y., Wallace, J. M., & Francis, R. C. (1997). Pacific interdecadal climate oscillation with impacts on salmon production. *Am. Meteorol. Soc*, *78*(6), 1069–1079. https://doi.org/10.1175/1520-0477(1997)078<1069:apicow>2.0.co;2

McCabe, G. J., Palecki, M. A., & Betancourt, J. L. (2004). Pacific and Atlantic Ocean influences on multidecadal drought frequency in the United States. *Proceedings of the National Academy of Sciences of the United States of America*. https://doi.org/10.1073/pnas.0306738101

McCabe, G. J., Betancourt, J. L., Gray, S. T., Palecki, M. a., & Hidalgo, H. G. (2008). Associations of multi-decadal sea-surface temperature variability with US drought. *Quaternary International*, *188*(1), 31–40. https://doi.org/10.1016/j.quaint.2007.07.001

Mo, K. C., Schemm, J. E., & Yoo, S. H. (2009). Influence of ENSO and the atlantic multidecadal oscillation on drought over the United States. *Journal of Climate*, *22*(22), 5962–5982. https://doi.org/10.1175/2009JCLI2966.1

NCDC, cited 2013: State of the climate: Drought–annual 2012. National Oceanic and Atmospheric Administration. [Available online at http://www.ncdc.noaa.gov/sotc/drought/]

Nigam, S., Guan, B., & Ruiz-Barradas, A. (2011). Key role of the Atlantic Multidecadal Oscillation in 20th century drought and wet periods over the Great Plains. *Geophysical Research Letters*, *38*(16), 1–6. https://doi.org/10.1029/2011GL048650

Niu, G. Y., Yang, Z. L., Mitchell, K. E., Chen, F., Ek, M. B., Barlage, M., … Xia, Y. (2011). The community Noah land surface model with multiparameterization options (Noah-MP): 1. Model description and evaluation with local-scale measurements. *Journal of Geophysical Research Atmospheres*, *116*(12), 1–19. https://doi.org/10.1029/2010JD015139

Oglesby, R., Feng, S., Hu, Q., & Rowe, C. (2012). The role of the Atlantic Multidecadal Oscillation on medieval drought in North America: Synthesizing results from proxy data and climate models. *Global and Planetary Change*, *84–85*, 56–65. https://doi.org/10.1016/j.gloplacha.2011.07.005

Otto-Bliesner, B. L., Brady, E. C., Fasullo, J., Jahn, A., Landrum, L., Stevenson, S., … Strand, G. (2016). Climate variability and change since 850 ce an ensemble approach with the community earth system model. *Bulletin of the American Meteorological Society*, *97*(5), 787–801. https://doi.org/10.1175/BAMS-D-14-00233.1

Pal, J. S., & Eltahir, E. A. B. (2001). Pathways relating soil moisture conditions to future summer rainfall within a model of the land-atmosphere system. *Journal of Climate*, *14*(6), 1227–1242. https://doi.org/10.1175/1520-0442(2001)014<1227:PRSMCT>2.0.CO;2

Palmer, W. C. (1965). Meteorological Drought. *U.S. Weather Bureau, Res. Pap. No. 45*. Retrieved from https://www.ncdc.noaa.gov/temp-and-precip/drought/docs/palmer.pdf

Rayner, N. A., Parker, D. E., Horton, E. B., Folland, C. K., Alexander, L. V., Rowell, D. P., … Kaplan, A. (2003). Global analyses of sea surface temperature, sea ice, and night marine air temperature since the late nineteenth century. *Journal of Geophysical Research*, *108*(D14), 4407. https://doi.org/10.1029/2002JD002670

Rippey, B. R. (2015). The U.S. drought of 2012. *Weather and Climate Extremes*, *10*, 57–64. https://doi.org/10.1016/j.wace.2015.10.004

Ropelewski, C. F., & Halpert, M. S. (1986). North american precipitation and temperature patterns associated with the El Nino/Southern Oscillation (ENSO). *Monthly Weather Review*. https://doi.org/10.1175/1520-0493(1986)114<2352:napatp>2.0.co;2

Ruprich-Robert, Y. *et al.* Assessing the climate impacts of the observed atlantic multidecadal variability using the GFDL CM2.1 and NCAR CESM1 global coupled models. *J. Clim.* **30,** 2785–2810 (2017).

Sarachik, E., and M. A. Cane, 2010: The El Niño–Southern Oscillation Phenomenon. Cambridge University Press

Schubert, S. D., Suarez, M. J., Pegion, P. J., Koster, R. D., & Bacmeister, J. T. (2004). Causes of long-term drought in the U.S. Great Plains. *Journal of Climate*, *17*(3), 485–503. https://doi.org/10.1175/1520-0442(2004)017<0485:COLDIT>2.0.CO;2

Schubert, S. D., Suarez, M. J., Pegion, P. J., Koster, R. D., & Bacmeister, J. T. (2008). Potential predictability of long-term drought and pluvial conditions in the U.S. Great Plains. *Journal of Climate*, *21*(4), 802–816. https://doi.org/10.1175/2007JCLI1741.1

Schubert, S., Gutzler, D., Wang, H., Dai, A., Delworth, T., Deser, C., … Zeng, N. (2009). A U.S. Clivar project to assess and compare the responses of global climate models to drought-related SST forcing patterns: Overview and results. *Journal of Climate*, *22*(19), 5251–5272. https://doi.org/10.1175/2009JCLI3060.1

Seager, R., & Hoerling, M. (2014). Atmosphere and ocean origins of North American droughts. *Journal of Climate*, *27*(12), 4581–4606. https://doi.org/10.1175/JCLI-D-13-00329.1

Seager, R., Kushnir, Y., Herweijer, C., Naik, N., & Velez, J. (2005). Modeling of tropical forcing of persistent droughts and pluvials over western North America: 1856-2000. *Journal of Climate*, *18*(19), 4065–4088. https://doi.org/10.1175/JCLI3522.1

Steiger, N. J., Smerdon, J. E., Cook, E. R., & Cook, B. I. (2018). A reconstruction of global hydroclimate and dynamical variables over the Common Era. *Scientific Data*, *5*, 1–15. https://doi.org/10.1038/sdata.2018.86

Steinman, B. A., Abbott, M. B., Mann, M. E., Stansell, N. D., & Finney, B. P. (2012). 1,500 year quantitative reconstruction of winter precipitation in the Pacific Northwest. *Proceedings of the National Academy of Sciences*, *109*(29), 11619–11623. https://doi.org/10.1073/pnas.1201083109

Stevenson, S., Timmermann, A., Chikamoto, Y., Langford, S., & DiNezio, P. (2015). Stochastically Generated North American Megadroughts. *Journal of Climate*, *28*(5), 1865–1880. https://doi.org/10.1175/JCLI-D-13-00689.1

Sutton, R. T., & Hodson, D. L. R. (2005). Atlantic Ocean Forcing of North American and European Summer Climate. *Science*, *309*(5731), 115–118. https://doi.org/10.1126/science.1109496

Sutton, R. T., & Hodson, D. L. R. (2007). Climate response to basin-scale warming and cooling of the North Atlantic Ocean. *Journal of Climate*, *20*(5), 891–907. https://doi.org/10.1175/JCLI4038.1

Trenberth, K. E., & Guillemot, C. J. (1996). Physical processes involved in the 1988 drought and 1993 floods in north America. *Journal of Climate*. https://doi.org/10.1175/1520-0442(1996)009<1288:PPIITD>2.0.CO;2

Taylor, K. E., Stouffer, R. J. & Meehl, G. A. An overview of CMIP5 and the experiment design. *Bull. Am. Meteorol. Soc.* **93,** 485–498 (2012).

Wang-Erlandsson, L., Van Der Ent, R. J., Gordon, L. J., & Savenije, H. H. G. (2014). Contrasting roles of interception and transpiration in the hydrological cycle - Part 1: Temporal characteristics over land. *Earth System Dynamics*, *5*(2), 441–469. https://doi.org/10.5194/esd-5-441-2014

Wang, S., Huang, J., He, Y., & Guan, Y. (2015). Combined effects of the Pacific Decadal Oscillation and El Niño-Southern Oscillation on Global Land Dry–Wet Changes. *Scientific Reports*, *4*(1), 6651. https://doi.org/10.1038/srep06651

Williams, A., Cook, B. I., Smerdon, J. E., Bishop, D. A., Seager, R., & Mankin, J. S. (2017). The 2016 Southeastern U.S. Drought: An Extreme Departure From Centennial Wetting and Cooling. *Journal of Geophysical Research: Atmospheres*, *122*(20), 10,888-10,905. https://doi.org/10.1002/2017JD027523

Wise, E. K., Wrzesien, M. L., Dannenberg, M. P., & McGinnis, D. L. (2015). Cool-season precipitation patterns associated with teleconnection interactions in the United States. *Journal of Applied Meteorology and Climatology*, *54*(2), 494–505. https://doi.org/10.1175/JAMC-D-14-0040.1

Xue, Y., Zeng, F. J., Mitchell, K. E., Janjic, Z., & Rogers, E. (2001). The impact of land surface processes on simulations of the US hydrological cycle: A case study of the 1993 flood using the SSiB land surface model in the NCEP Eta regional model. *Monthly Weather Review*, *129*(12), 2833–2860. https://doi.org/10.1175/1520-0493(2001)129<2833:TIOLSP>2.0.CO;2

Yang, Y. S. Xie, L. Wu, Y. Kosoka, & Li, J. (2017). ENSO forced and local variability of North Tropical Atlantic SST: model simulations and biases. *Climate Dynamics*, https://doi.org/ 10.1007/s00382-017-3679-9

Yu, B., & Zwiers, F. W. (2007). The impact of combined ENSO and PDO on the PNA climate: A 1,000-year climate modeling study. *Climate Dynamics*, *29*(7–8), 837–851. https://doi.org/10.1007/s00382-007-0267-4

Table 1. Sensitivity of model results to the pan-CONUS spatial extent threshold. The number of pan-CONUS droughts, the percent ocean contribution, and the percent atmospheric variability contribution are given for spatial thresholds of increasing percentages of the CONUS under drought for CAM5 and CCM3 GOGA, CCM3 POGA-ML, and CCM3 TAGA ensembles.

Spatial Extent Threshold (% Area)	Number of Droughts	Ocean Contribution	Atmospheric Variability Contribution
CCM3 GOGA			
50	277	53%	47%
55	142	52%	48%
60	74	48%	52%
65	34	45%	55%
70	9	45%	55%
CCM3 POGA-ML			
50	248	46%	54%
55	128	45%	55%
60	53	42%	58%
65	13	36%	64%
70	2	29%	71%
CCM3 TAGA			
50	189	15%	85%
55	82	15%	85%
60	33	15%	85%
65	10	20%	80%
70	4	22%	78%
CAM5 GOGA			
50	303	39%	61%
55	161	37%	63%
60	88	32%	68%
65	44	31%	69%
70	16	27%	73%
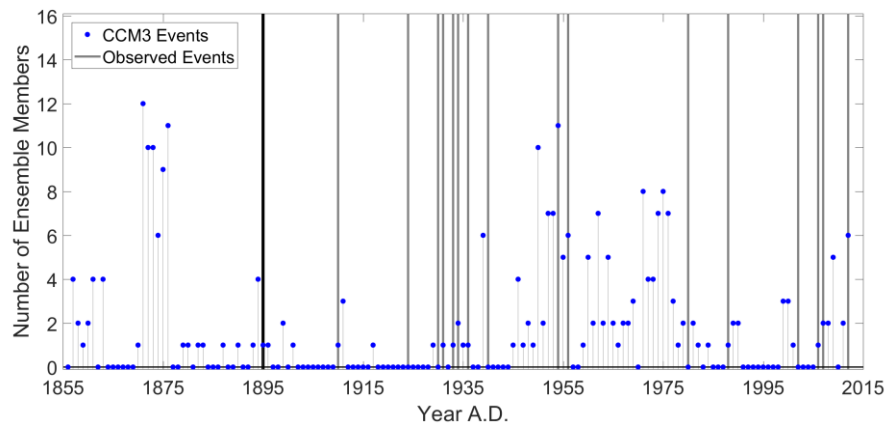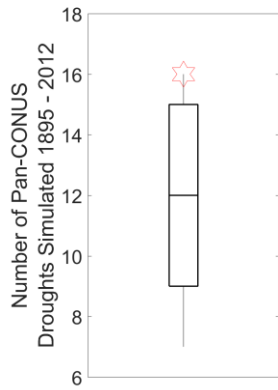
Figure 1. (left) Boxplot of the number of pan-CONUS droughts simulated (7 to 16) in the CCM3 GOGA ensemble from 1895 – 2012. Red star indicates the number of pan-CONUS droughts (16) identified in the MCDI data. (right) Time series of the number of ensemble members simulating pan-CONUS droughts each year from 1856 to 2012 CCM3 GOGA. Gray lines represent identified pan-CONUS droughts in the observational-based MCDI data. Black solid line at 1895 marks the beginning of observational data availability.
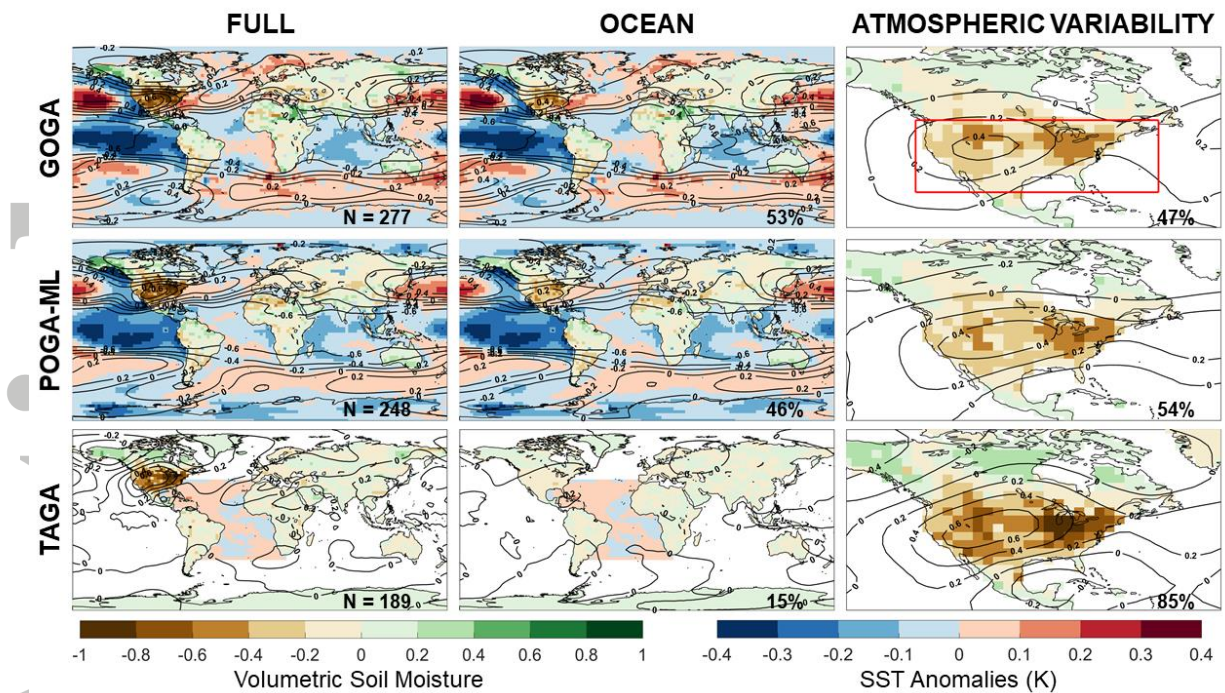
Figure 2. (left column) Composite of all pan-CONUS droughts (as estimated from volumetric soil moisture at 80 cm) and their associated annual SST and 500mbar anomalies from 1856-2007 across the 16-member (top row) CCM3 GOGA, (middle row) CCM3 POGA-ML, and (bottom row) CCM3 TAGA ensembles. The sample size in the composite is given in bottom right corner. (middle column) The ocean contribution to the pan-CONUS drought composite. The percent contribution of the ocean to the severity of pan-CONUS droughts is given in bottom right corner. (right column) The internal atmospheric contribution to the pan-CONUS drought composite. The percent contribution of internal atmospheric variability to the severity of pan-CONUS droughts is given in bottom right corner. Red box in top right panel represents our study region ($24.5 - 49°N$ to $59.5 - 127°W$).
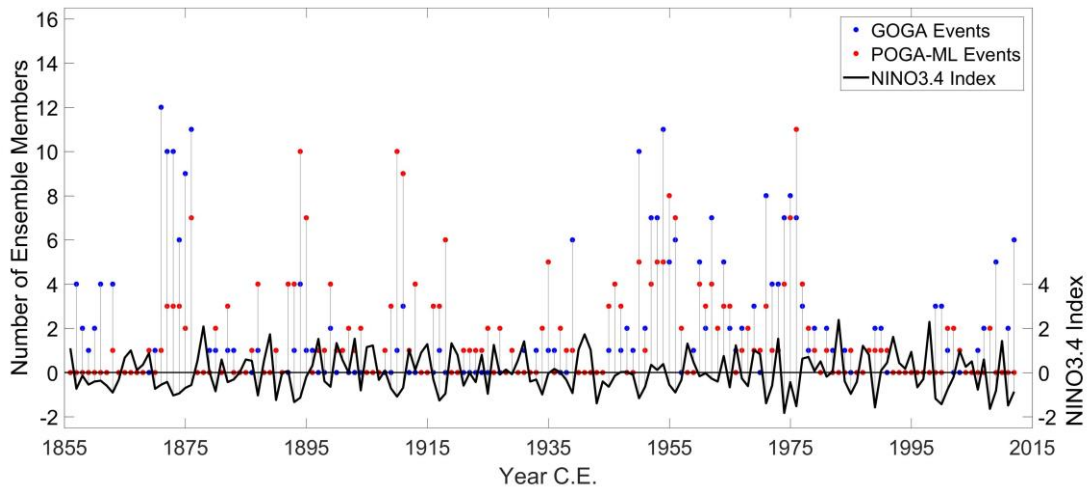
Figure 3. Time series of the NINO3.4 index and the number of ensemble members simulating pan-CONUS drought each year from 1856 to 2012 for the CCM3 GOGA and POGA-ML configurations.
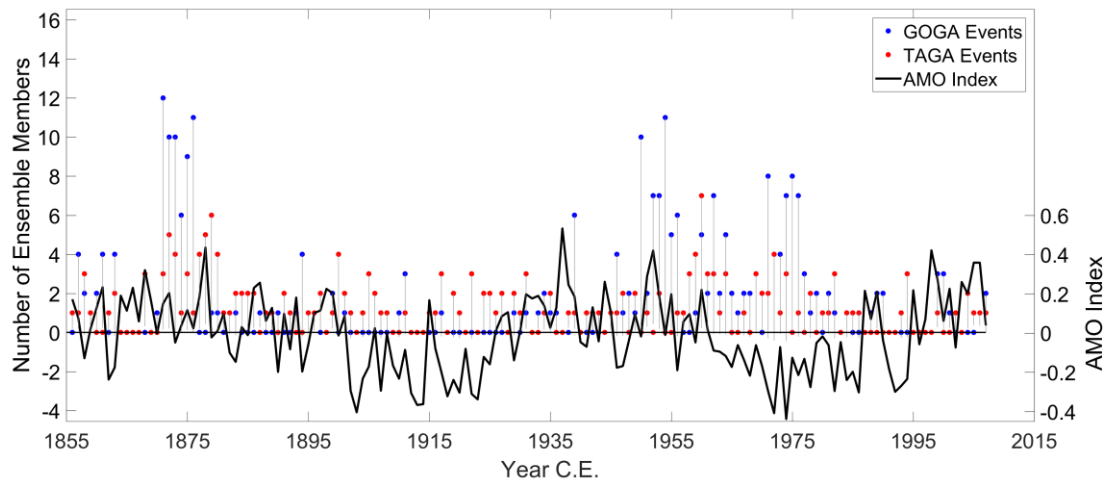
Figure 4. Time series of the AMO index and the number of ensemble members simulating pan-CONUS droughts each year from 1856 to 2007 for the CCM3 GOGA and TAGA configurations.
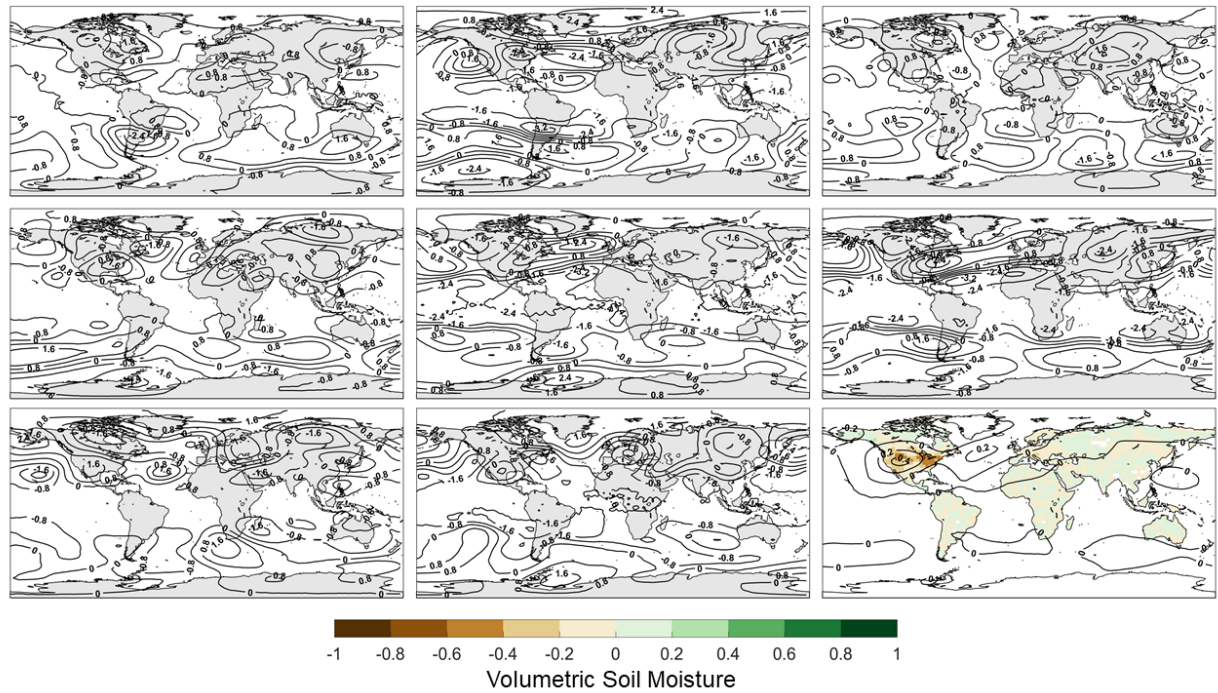
Figure 5. Global plots of 8 individual internal atmospheric variability contributions to pan-CONUS droughts and their associated annual 500mbar geopotential height anomalies from the CCM3 GOGA 16-member ensemble. The composite of the same field and for soil moisture for all pan-CONUS droughts from the CCM3 GOGA 16-member ensemble is given in the bottom right panel.
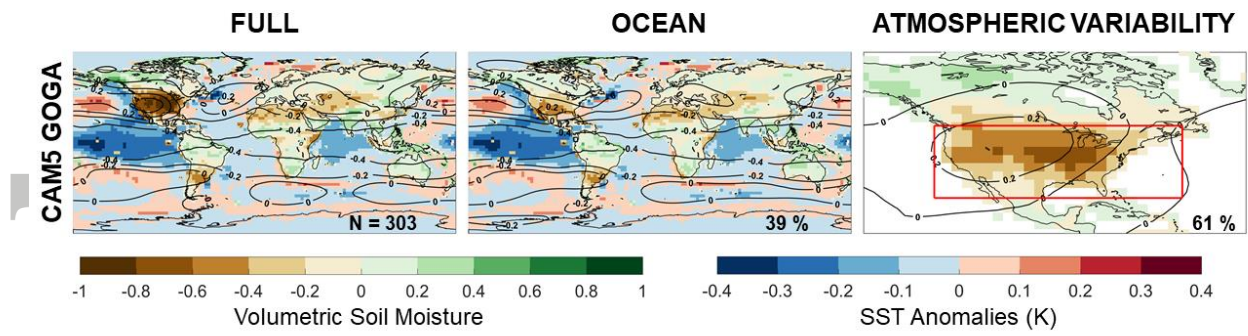
Figure 6. Same as top row of Figure 2, but for the CAM5 GOGA experiment. Red box in top right panel represents our study region (24.5 – 49°N to 59.5 – 127°W).
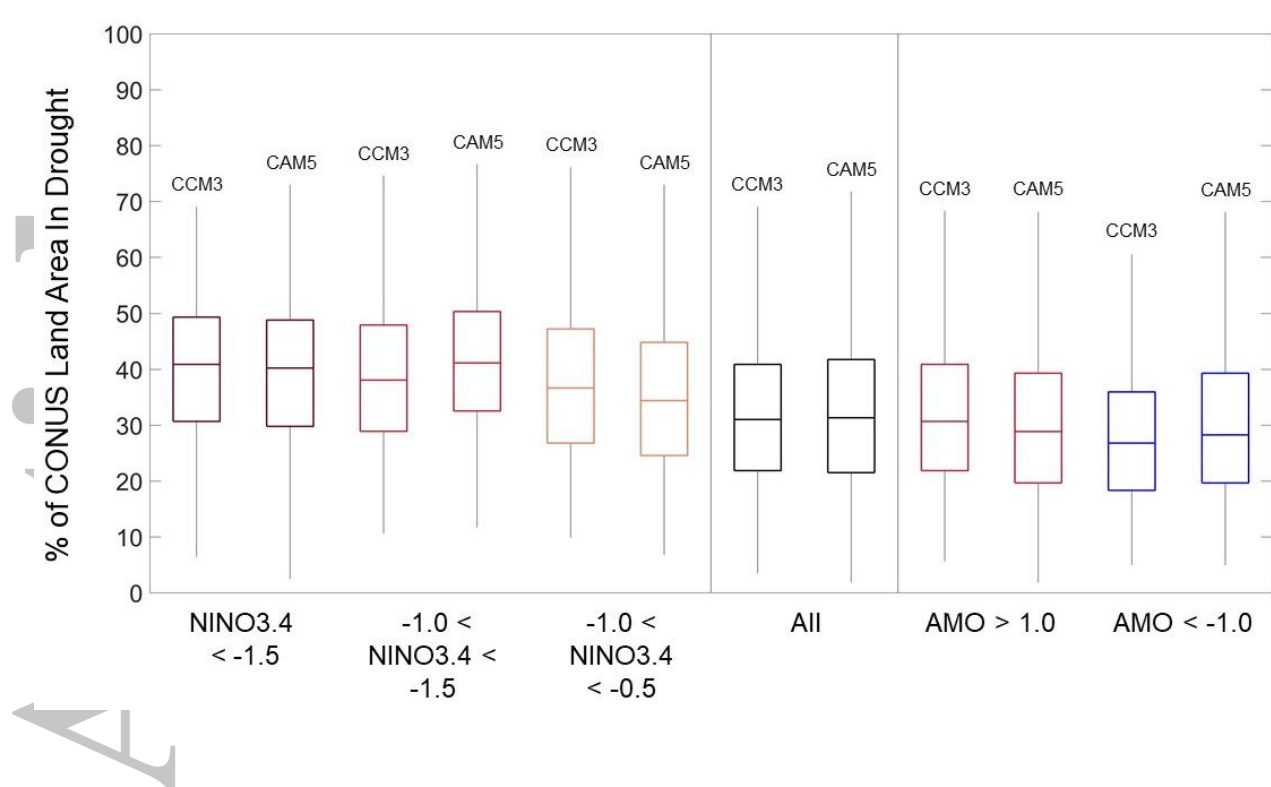
Figure 7. CCM3 and CAM5 GOGA ensemble aggregate boxplots of the percent of CONUS under drought between 1856 – 2012 under various ENSO and AMO conditions (standard deviations above the mean).
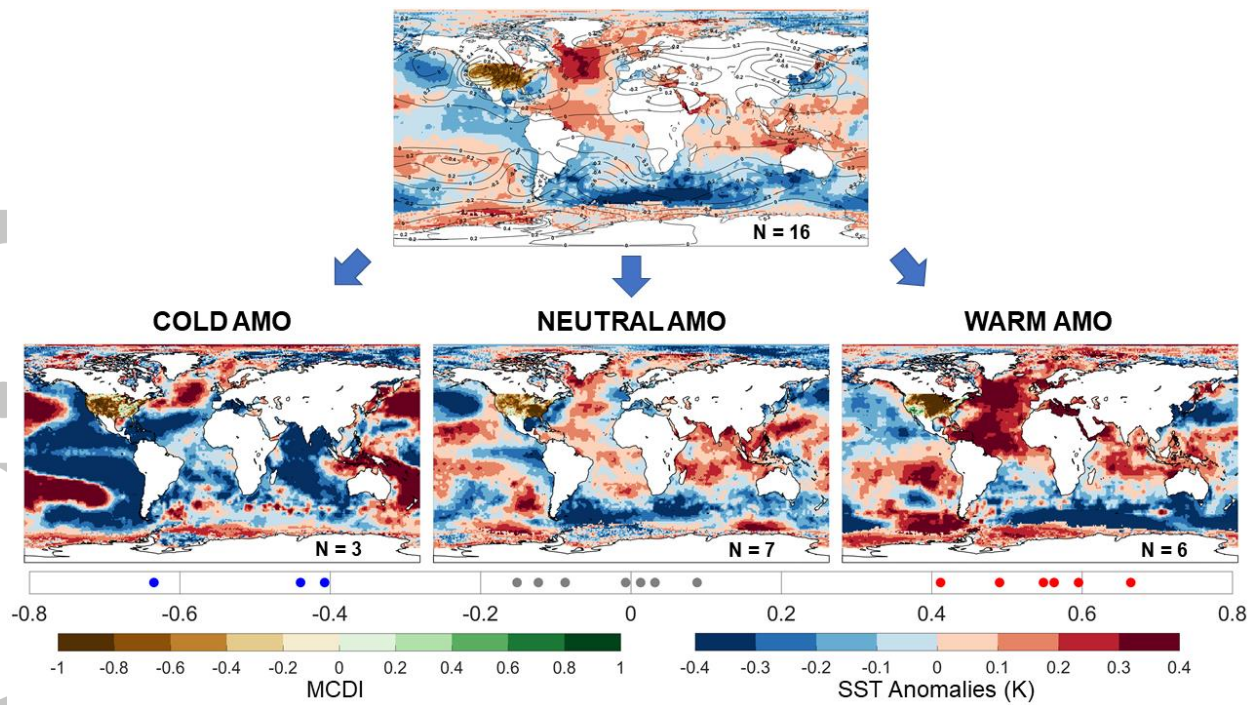
Figure 8. (top) Composite of pan-CONUS droughts (N = 16) in observation-based MCDI data and their associated SST and geopotential height over the 1895 – 2014 interval. The pan-CONUS drought years are: 1910, 1924, 1930, 1931, 1933, 1934, 1936, 1940, 1954, 1956, 1980, 1988, 2002, 2006, 2007, and 2012. (bottom) Observed pan-CONUS drought composites based on their AMO index. The number of years is shown in the bottom right corner of each map composite. The AMO index values for each of the 16 observed pan-CONUS droughts in each of their respective groupings are shown underneath the observed composite maps. 1910, 1956, and 2002 are cold AMO years. 1924, 1930, 1940, 1954, 1980, 1988, and 2007 are neutral AMO years. 1931, 1933, 1934, 1936, 2006, and 2012 are warm AMO years.
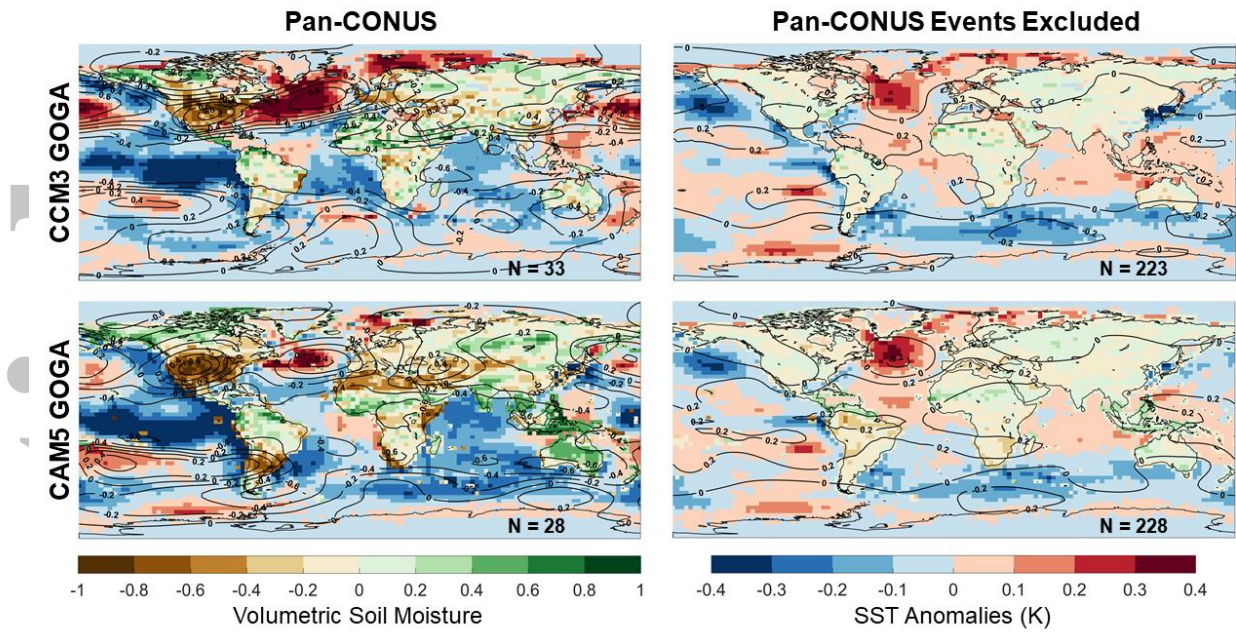
Figure 9. (top row) CAM5 and (bottom row) CCM3 GOGA ensemble composites of (i) pan-CONUS droughts and (ii) remaining years excluding pan-CONUS droughts from only the subset of years in which pan-CONUS droughts occurred in the observational record. The number of years is shown in the bottom right corner of each map.